International Journal of Electrical and Computer Engineering (IJECE)
Vol. 15, No. 4, August 2025, pp. 3649~3659
ISSN: 2088-8708, DOI: 10.11591/ijece.v15i4.pp3649-3659

Numerical modelling of photocurrent for CuInxGa1-xSe2-based bifacial photovoltaic cell

Seloua Bouchekouf[1], Hocine Guentri[2], Liamena Hassinet[1], Amina Merzougui[1], Farida Kebaili[3]
[1]Instiue of Science and Technology Department of Mechanical and Electromechanical Engineering, University Centre Abdelhafid Boussouf, Mila, Algeria
[2]Department of Electrical Engineering, Institute of Technologies, Laboratory of Electronic Systems, Telecommunications and Renewable Energies, University Center Nour Bachir El Bayadh, El Bayadh, Algeria
[3]Department of Electronics, Faculty of Technology, Laboratory of Signals and Systems Analysis University of M'sila, M'sila, Algeria

Article Info

Article history:

Received Oct 9, 2024
Revised Apr 6, 2025
Accepted May 24, 2025

Keywords:

Absorption coefficient
Back surface field
Bifacial photovoltaic cell
Conversion efficiency
P+ doped layer
Photocurrent

ABSTRACT

Research on thin-film solar cells based on $CuInSe_2$ has demonstrated the potential of this compound for photovoltaic conversion. The introduction of gallium as a substitute for indium has led to the creation of the $CuIn_xGa_{1-x}Se_2$ (CIGS) structure, which could serve as one of the foundational materials for high-performance solar cells. This paper focuses on modelling the bifacial back surface field (BSF) solar cell. We took the CdS/CIGS thin-film structure as an application example to optimize, through simulation, the physical-electronic and geometric parameters of the various layers of the cell. Our study has led us to interesting results that clearly show that the performance of the cell is precisely controlled by the space charge region associated with the CIGS absorber layer, which is promising for research in photovoltaics due to its high absorption coefficient and the ability to vary its bandgap, allowing for increased conversion efficiency. The high-doped P+ layer (Wbsf) enhances the total photocurrent of the bifacial.

This is an open access article under the CC BY-SA license.

Corresponding Author:

Hocine Guentri
Department of Electrical Engineering, Institute of Technologies, Laboratory of Electronic Systems, Telecommunications and Renewable Energies, University Center Nour Bachir El Bayadh
El Bayadh, Algeria
Email: h.guentri@cu-elbayadh.dz

1. INTRODUCTION

The development of research on crystalline structures with a direct bandgap (high α) allows for a shift towards thin-film cells, whether amorphous or polycrystalline. Their main advantages lie in their stability and the variety of deposition techniques available. Among this approach's most commonly used materials are I-III-VI2 type compounds such as $CuInSe_2$, which has a very high α (10^5 cm^{-1}). However, the bandgap value of CIS (1.02 eV) is quite far from the optimum value for photovoltaic conversion. This is increased using the quaternary alloy $CuIn_xGa_{1-x}Se_2$ (CIGS) [1], [2], which forms the basis of the CdS/CIGS cell we will study in this article.

The solar cell's back surface (total metallization) is characterized by a very high surface recombination velocity. Installing a back surface field (BSF) involves creating a potential barrier (p+-p junction) on the rear face to ensure passivation. Thus, adding an electric field at the back surface near the ohmic contact causes minority carriers to be pushed towards the space charge region for better collection [3].

Recently, investigators have examined the efficiency of CIGS-based bifacial photovoltaic cells, like Shin *et al.* [4] propose a semi-transparent and bifacial ultrathin Cu(In, Ga)Se_2 solar cells via a single-stage process and light-management strategy. Also, Salhi [5] present the principles and technologies to manufacture the photovoltaic cell based on CIGS. Furthermore, Violas *et al.* [6] address the impact of a transparent conducting oxide layer used as rear contact in CIGS solar cells. Furthermore, Soheili *et al.* [7] propose a novel multi-junction CGS/CIGS solar cell. Moreover, Mufti *et al.* [8] review the CIGS solar cells from the point of view of structural engineering. Rawat *et al.* [9] make use of CIGS-based solar cells due to their high absorption coefficient, stability, and affordability.

The interest of this work is to improve the efficiency of a photovoltaic cell by increasing the value of the photocurrent delivered by this cell. Using a bifacial cell captures solar radiation and the collection of carriers by both sides of the cell on the one hand. On the other hand, the cell is based on the CIGS quaternary, which has a very high absorption and a possibility of adjusting the Ug2 gap value around the optimal value (1.35 eV) for photovoltaic conversion. This paper focuses on the modelling of the bifacial BSF solar cell. We took the CdS/CIGS thin-film structure as an application example. And we performed several tests on this structure.

2. CRYSTALLINE STRUCTURE OF CIGS

CIGS is among the solid solutions $A(B'_{1-x}B''_{x})\,X_2$, obtained by introducing gallium (Ga) into CIS ($CuInSe_2$) as a substitute for indium (In) [10], [11]. A semiconductor $A^{N-1}B^{\,N+1}X_2^{8-N}$ arises from the substitution, in a binary $C^NX^{\,8-N}$ crystallized zinc blende, of cations C from column N by those A and B from columns N-1 and N+1. In group I, N-1=1, thus N=2 and N+1=3; this group belongs to the family of semiconductors known as II-VI [12].

The ternary components Cu-III-VI_2 crystallize in two allotropes. The first, which is of the sphalerite (zinc blende) type, occurs at high temperatures (T > 810 °C). The second, of the chalcopyrite type (anomaly of the blende), occurs at temperatures below 665 °C [13] with an ordered tetragonal structure. These structures are represented in Figure 1. $CuInSe_2$ and $CuGaSe_2$, which form the alloy Cu(In, Ga)Se_2, belong to group I and crystallize in the chalcopyrite structure [14].

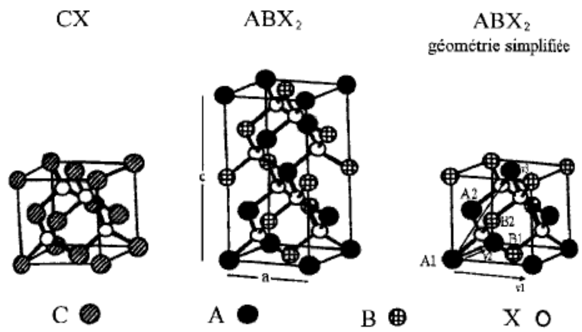

Figure 1. Two allotropic forms of the Cu-III-VI_2 elemental lattice: Blende-type sphalerite structure and chalcopyrite structure [13]

3. OPTICAL PROPERTIES OF CIGS

CIGS is a semiconductor material commonly used in thin-film photovoltaic cells. It exhibits several notable optical properties that make it highly efficient for solar energy conversion. Here is an overview of its key optical properties.

3.1. The bandgap Ug

The gap of the $CuIn_{1-x}Ga_xSe_2$ quaternary varies from 1 eV (x=0) to 1.7 eV (x=1). This material's advantage is that it allows the gap value and crystallographic parameters to be adjusted to approach the optimum gap value (around 1.35 eV) for photovoltaic conversion and ensure better mesh matching between the two materials in a heterojunction [15], [16].

3.2. The absorption coefficient

The absorber material's optical absorption coefficient is a fundamental parameter. For ternary $CuInSe_2$ (CIS), $CuGaSe_2$ (CGS) and quaternary Cu(In, Ga)Se_2 (CIGS), the absorption coefficient is very high, on the order of 10^4 cm^{-1} above their gap [1]. Figure 2 shows the α(hν) curve of frequently used materials. $CuInSe_2$ has the highest absorption coefficient compared to photovoltaic materials currently used [17].

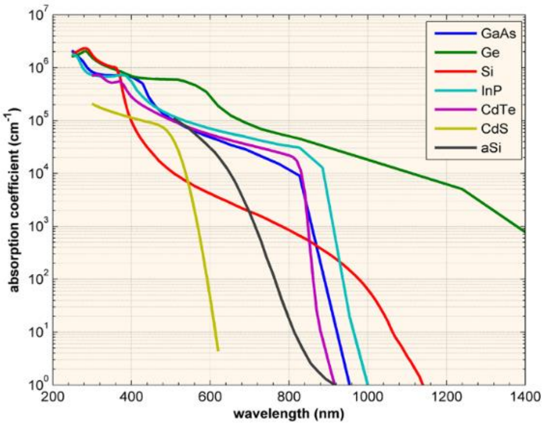

Figure 2. Variation in the optical absorption coefficient of absorber materials [18]

4. THE CdS/CIGS SOLAR CELL

The CdS/CIGS photovoltaic cell has a "thin-film" structure, with a stack of films no more than a few microns thick. Its standard structure includes a back electrode consisting of a substrate on which a thin metal layer is deposited as a contact. The absorber layer, Cu(In, Ga)Se_2, has a high absorption coefficient and an optimum direct gap of 1.5 eV. A CdS or ZnO buffer layer, 10 to 100 nm thick, provides the junction and prevents short circuits. Finally, an aluminum-doped ZnO optical window and a Ni/Al/Ni gate complete the cell, guaranteeing conductivity and transparency while connecting the cell to the external circuit Figure 3 [19].

The bifacial cell allows illumination from both sides. However, illumination from the rear offers inferior performance to that from the front. These cells exploit light reflected from the ground, thanks to their double-sided design. Figure 4 shows the semi-transparent in Figure 4(a) and bifacial solar cell based on CIGS in Figure 4(b).

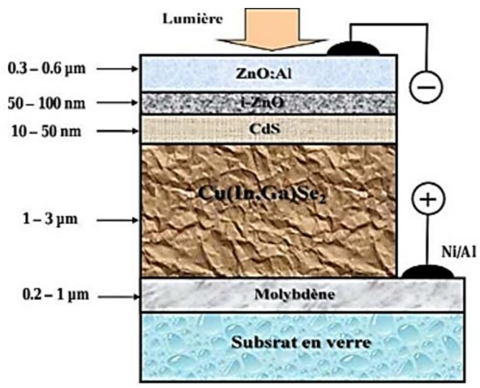

Figure 3. The structure of the ZnO/CdS/Cu(In,Ga)Se_2 thin-film cell [19]

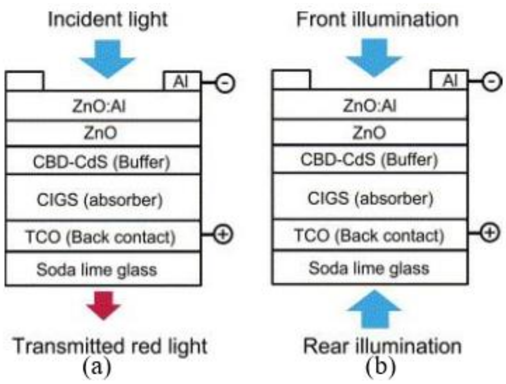

Figure 4. Solar cell based on CIGS: (a) semi-transparent and (b) bifacial [20]

5. THE BSF THEORY

The losses generated by defects and ohmic contacts on both surfaces of a solar cell are modelled by surface recombination, characterized by a velocity that reflects the quality of the surfaces. To tackle this problem, research has focused on solar cell structures designed to reduce these losses. The simplest configuration in this field is the back surface field (BSF) bifacial cell, which allows the rear surface to capture light reflected from the ground [21] as shown in Figure 5.

The solar cell base comprises two regions: the base itself and a heavily doped zone near the back contact. This has two consequences: creating a small additional energy barrier and the confinement of minority carriers to the base Figure 5. In this way, we recover the charge carriers created at the back of the base near the ohmic contact, normally lost in single cells. Figure 6 shows the energetic structure of the BSF solar cell with minority carrier confinement.

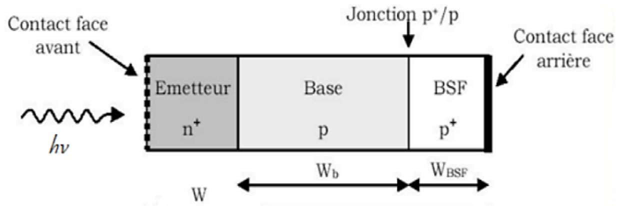

Figure 5. Solar cell with BSF field [21]

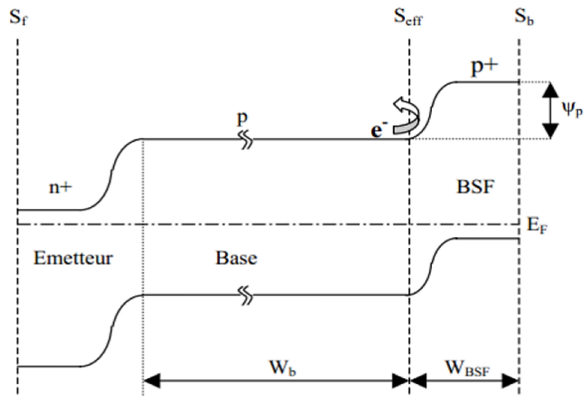

Figure 6. Band diagram of a BSF solar cell [22]

6. CALCULATION OF PHOTOCURRENT AND I(V) CHARACTERISTICS

To obtain the cell's output characteristics, we first had to calculate the photocurrent supplied by the cell. From the continuity and current equations, we determined the distribution of carriers along the cell and derived the equation that characterizes the photocurrent. We approached the one-dimensional model Figure 7, based on four regions: the N+ zone (the emitter), the P zone (the base), the space charge zone (ZCE) and the heavily doped zone (P+) [23].

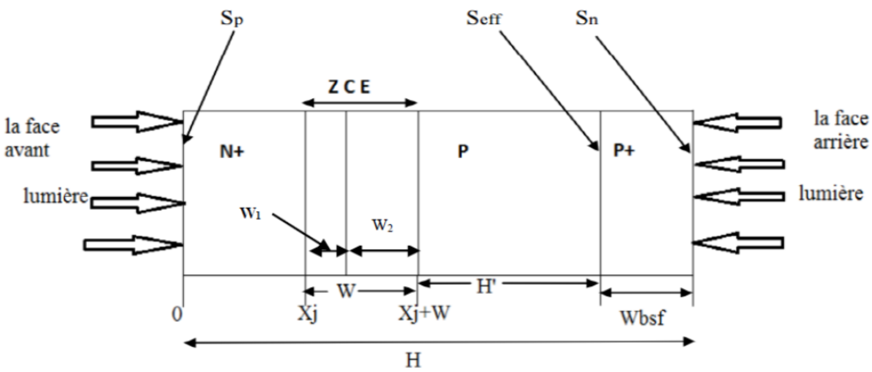

Figure 7. Geometry of the bifacial solar cell [23]

By numerically solving the continuity and current equations using the iterative method, we determined the distribution of carriers along the cell. We deduced the equation that characterizes the current for each point of the cell. Our comprehensive approach to determining the total photo-current density produced by the bifacial cell J_{ph}, which is equal to the sum of the photo-currents generated in each region of the cell, ensures the accuracy of our findings.

$$J_{ph} = J_n + J_p + J_{ZCE} + J_{bsf} \quad (1)$$

– Continuity equations [24]:

$$\frac{\partial n}{\partial t} = G_n - \frac{\Delta n}{\tau_n} + \frac{1}{q} div(Jn) \tag{2}$$

$$\frac{\partial p}{\partial t} = G_p - \frac{\Delta p}{\tau_p} - \frac{1}{q} div(Jp) \tag{3}$$

– Current equations:

$$Jn = q\mu_n nE + \mu_n KT \frac{\partial n}{\partial x} \tag{4}$$

$$Jp = q\mu_p pE - \mu_p KT \frac{\partial p}{\partial x} \tag{5}$$

6.1. Calculation of current in CdS (n)

This layer gives us a photohole (Ip) expressed by (8).

– Boundary conditions:

$$S_p \Delta_p = D_p \frac{\partial \Delta p}{\partial x}\Big|_{x=0} \tag{6}$$

(S_p: recombination speed at the surface)

$$\Delta p|_{x=x_j} = 0 \tag{7}$$

$$Jp = \frac{q\alpha_1 L_p \Phi_i (1-R)}{(\alpha_1^2 L_p^2 - 1)} \left[\frac{\left(\frac{S_p L_p}{D_p} + \alpha_1 L_p\right) - exp(-\alpha_1 x_j)\left(\frac{S_p L_p}{D_p} cosh\left(\frac{x_j}{L_p}\right) + sinh\left(\frac{x_j}{L_p}\right)\right)}{\frac{S_p L_p}{D_p} sinh\left(\frac{x_j}{L_p}\right) + cosh\left(\frac{x_j}{L_p}\right)} - \alpha_1 L_p \, exp(-\alpha_1 x_j) \right] \tag{8}$$

$$L_p = L_{Cds} \tag{9}$$

6.2. Current in the active zone (Ig=JZCE)

The carriers generated in the active zone (in the vicinity of the interface) are effective at dissociation (charge production), so the photocurrent in this zone is expressed by (10) [25]:

$$Jg = q\Phi_i (1-R) \, exp(-\alpha_1 x_j) \tag{10}$$

6.3. Calculation of current in CIGS (p)

This is the donor zone, giving us a photoelectron (In) [25]:

– Boundary conditions:

$$S_n \Delta_n = D_n \frac{\partial \Delta n}{\partial x}\Big|_{x=h} \tag{11}$$

(S_n: recombination speed at back contact, h= H- W_{bsf})

$$\Delta n|_{x=x_j+w1+w2} = 0 \tag{12}$$

$$Jn = \frac{q\Phi_i (1-R) \, exp(-\alpha_1(x_j+\omega_1)) \, exp(-\alpha_2\omega_2)\alpha_2 L_n}{(\alpha_2^2 L_n^2 - 1)} \left[\alpha_2 L_n - \frac{\frac{S_n L_n}{D_n}\left(cosh\left(\frac{x_b}{L_n}\right) - exp(-\alpha_2 x_b)\right) + sinh\left(\frac{x_b}{L_n}\right) + \alpha_2 L_n \, exp(-\alpha_2 x_b)}{\frac{S_n L_n}{D_n} sinh\left(\frac{x_b}{L_n}\right) + cosh\left(\frac{x_b}{L_n}\right)} \right] \tag{13}$$

$$L_n = L_{CIGS} \tag{14}$$

$$x_b = H - (x_j + w_1 + w_2 + w_{bsf}). \tag{15}$$

6.4. Photo current in the highly doped region P+

As with the base, for this region we used a layer of CIGS P+. The photo current generated is given by (16) [26].

$$J_{bsf} = -\left(\frac{qD_{bsf}}{L_{bsf}}\right)\left[\frac{N_a+N_e}{n_{bsf}} - n_p\right] + \cosh\left(\frac{w_{bsf}}{L_{bsf}}\right) \quad (16)$$

with N_a: acceptor concentration in the P region. n_p: electron concentration in the P region. N_e: electron concentration at x=H- $Wbsf$.

6.5. The effective recombination speed at the back face

The effective recombination speed at the back face of the BSF bifacial solar cell, illuminated by its back face, S_{eff} is given by (17) [26].

$$S_{eff} = \frac{N_a}{N_{bsf}}\frac{D_{bsf}}{L_{bsf}}\frac{\frac{S_n L_{bsf}}{D_{bsf}}+th(\frac{w_{bsf}}{L_{bsf}})}{1+\frac{S_n L_{bsf}}{D_{bsf}}th(\frac{w_{bsf}}{L_{bsf}})} \quad (17)$$

7. SIMULATION OF BIFACIAL CdS/CIGS CELL CHARACTERISTICS

Numerical simulation is commonly used for the optimization of solar cells. It is independent of the technology used and allows the different parameters to vary widely. Solar cell simulation using different simulators consists of understanding the behavior of these devices according to parameters such as thickness, gap and doping of regions on the characteristics of the solar cell (Icc, Vco, FF, η). In this step, we will present the numerical simulation results using MATLAB software. We took the CdS/CIGS thin-film structure as an application example to validate our physical model describing the BSF solar cell with:

– The emitter: doped type N $Nd.$ =10^{17}/cm^3 and thickness $Xj.$ = 50 nm.
– The base: doped type P Na=2×10^{16}/cm^3 and thickness Wb= 1.5 μm.
– The BSF layer: high-doped type P N_{BSF} = 8×10^{18}/cm^3 and thickness W_{BSF} = 0.7 μm.

7.1. Photocurrent presentation

In this section, we aim to present the BSF CdS/CIGS cell characteristics according to the model presented in Part 6 of this article. These results have been obtained by solving the continuity and current equations. Calculating this photo-current will enable us to determine these characteristics. We can observe in Figure 8 that the number of photons decreases exponentially, following the same variation pattern as the spectral distribution of solar radiation. The cell is susceptible to incident photons in the range of 0.3 µm to 0.75 µm, above which illumination becomes weak.

Figure 9 shows the dynamic variation of the absorption coefficient of the CdS emitter. The curve demonstrates a rapid change, with a considerable absorption reaching 10^4 cm^{-1} but over a very short interval. The nullity of the curve is from the value λ=0.5 µm, highlighting the dynamic nature of the material's behavior.

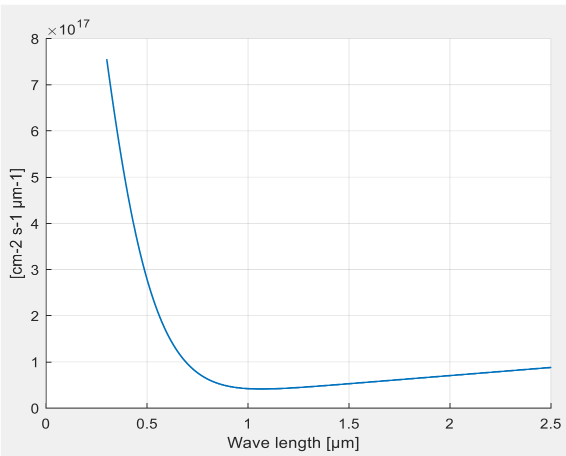

Figure 8. Number of incident photons as a function of wavelength

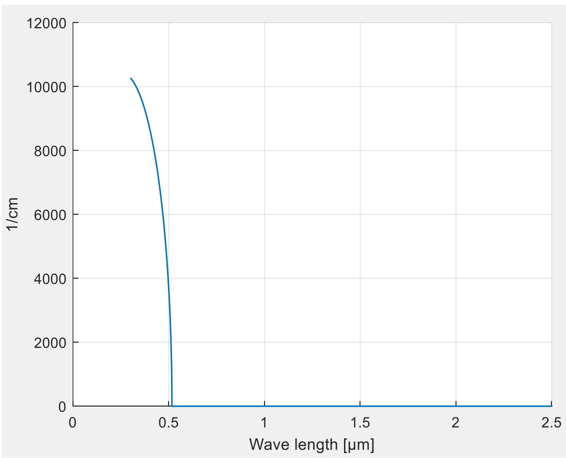

Figure 9. Absorption coefficient of CdS as a function of wavelength

Figure 10 shows the variation of the absorption coefficient of the CIGS base. The CIGS quaternary has a significant absorption > 4.5 10^4 cm^{-1} over a large interval extending to λ=1.25 µm. This absorption covers the range where the number of photons is intense. This is the advantage that this semiconductor represents for CIGS-based photovoltaic cells. The CdS photocurrent shown in Figure 11 with energetic excitations (the incident flux) varies according to the shape of the photon flux curve Figure 8 and the absorption coefficient Figure 9.

Figures 10 and 12 show the absorption coefficient and photo-current delivered by the CIGS base. The CIGS quaternary has a high absorption. This is the advantage that this semiconductor represents for CIGS-based photovoltaic cells because if we compare the current density it delivers with that delivered by CdS, we find that CIGS delivers a very high density, in addition to the advantage given by its wide absorption range and very high absorption coefficient.

Figure 13 shows the photocurrent delivered in the ZCE. This figure clearly shows that the photocurrent generation in this zone gives a high current for a very small thickness compared with that of the base due to the E field inside this zone. The shape of this curve is identical to that of the CIGS layer, indicating the predominance of the CIGS photocurrent density over that of CdS.

The results of the simulation presented in Figure 14, show that the highly doped layer introduces a significant current for a minimal thickness compared to the base. Also, the total photocurrent density produced by the Jph bifacial cell is equal to the sum of the photocurrents generated in each region of the cell shown in Figure 15. The addition of an electric field to the back surface in the vicinity of the ohmic contact means that minority carriers will be repelled toward the space charge zone, resulting in better collection.

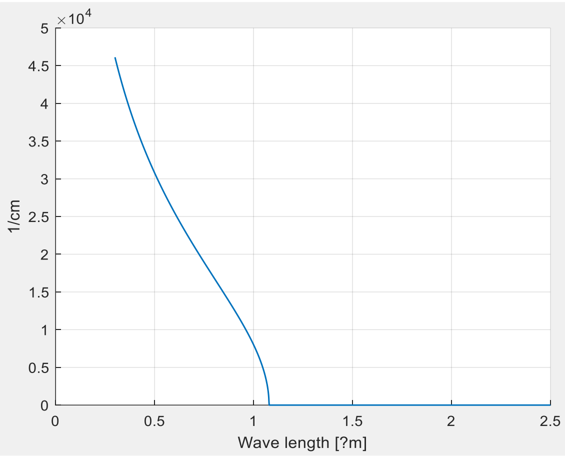

Figure 10. Absorption coefficient of CIGS as a function of wavelength

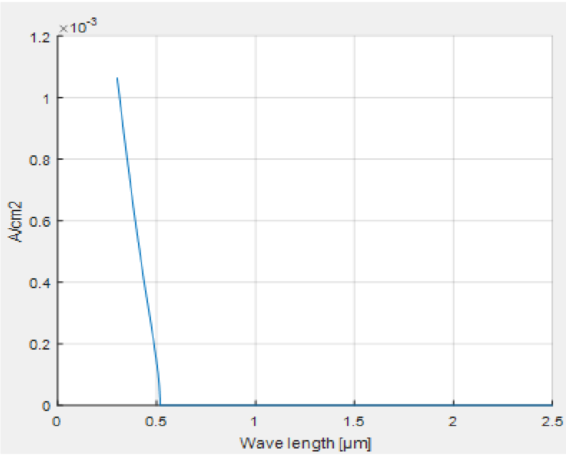

Figure 11. CdS emitter current density (hole current) as a function of wavelength

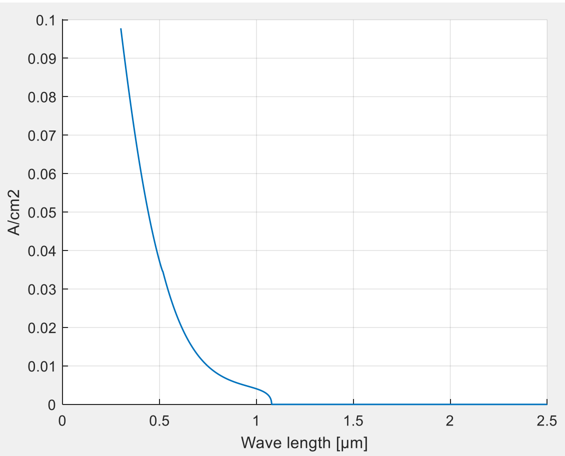

Figure 12. CIGS base current density as a function of wavelength

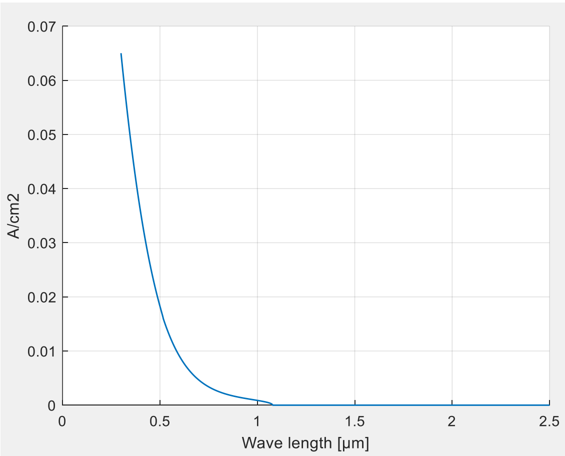

Figure 13. ZCE current density as a function of wavelength

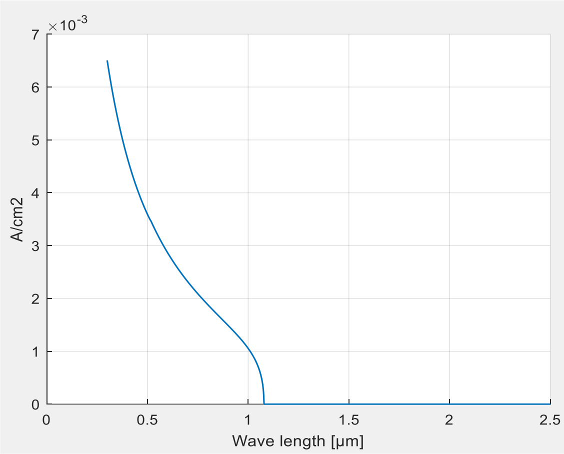

Figure 14. Back layer current density P+ as a function of wavelength

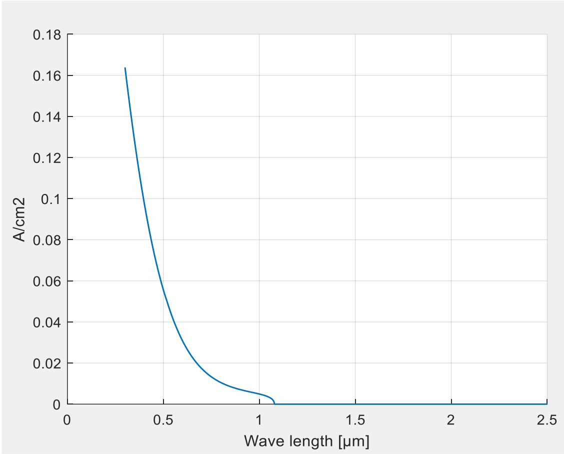

Figure 15. Total current density as a function of wavelength

7.2. Presentation of the I(V) and P(V) characteristics

Due to the nonlinearity of the output equation I(V) [24], its resolution is difficult. For this purpose, we use numerical resolution methods, utilizing a powerful software called MATLAB.

$$I(V) = I_{SC} - I_S\, exp\left(\frac{q(V+R_S I)}{kT}\right) \quad (18)$$

We will also present results that highlight the importance of this type of solar cell.

Figures 16 and 17 show an increase in the cell's output characteristics due to the photocurrent of the highly doped P+ zone. We have deduced the CdS/CIGS BSF solar cell parameters, which are grouped in Table 1. These results are compared with those of the conventional CdS/CIGS structure and with experimental results from NREL (National Renewable Energy Laboratory from the USA Department of Energy) Table 2.

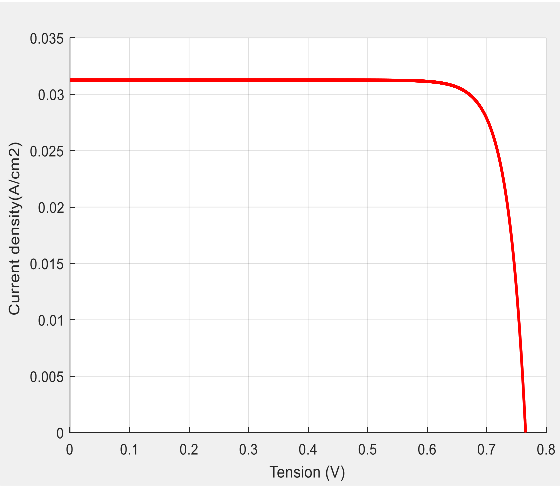

Figure 16. Output characteristic I(V) of the CdS/CIGS BSF cell

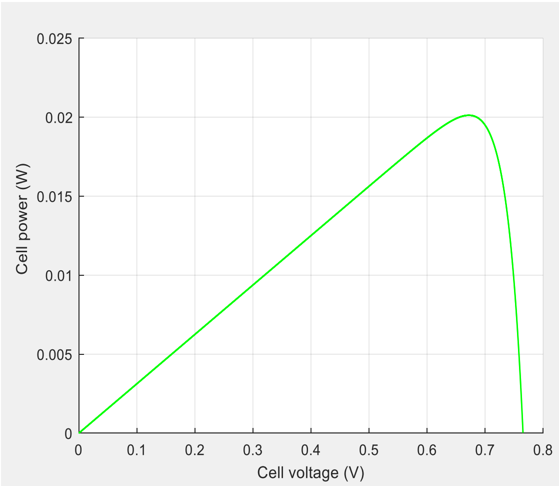

Figure 17. CdS/CIGS BSF cell power P(V) as a function of voltage

Table 1. Output characteristics of the CdS/CIGS cell

Parameters	I_{sc} (A/cm^2)	V_{c0} (v)	Efficiency (%)	FF (%)
Bifacial cell	0.0312	0.7310	21.8956	83.5628
conventional cell	0.0288	0.6022	19.3087	81.0869

Table 2. Output characteristics of the CIGS-based cell by NREL (National Renewable Energy Laboratory from the USA Department of Energy) [27]

Device Name	Sector (cm^2)	η (%)	Vco (mv)	FF (%)	Jsc(mA/cm^2)	Civil servant Measurement?
M2992-11#5	0.419	19.9	690	81.2	35.4	Yes

8. CONCLUSION

This work presents a simulation of the characteristics and performance of the bifacial CdS/CIGS thin-film photovoltaic cell obtained by solving the continuity and current equations. These equations model the photocurrent density exiting each of the four parts of the cell (emitter, base, ZCE, and P+ layer). The cell shows an optimum conversion efficiency η=22.39% for $Na=10^{15}$ cm^{-3}, $Nd=10^{17}$ cm^{-3}, and Ug2=1.15 eV.

The main results obtained show that: The operation of the BSF bifacial solar cell is the same as that of the conventional solar cell, with the addition of an electric field at the rear surface in the vicinity of the ohmic contact (the effect of the highly doped P+ layer). CIGS photocurrent density predominates over that of CdS. Photo generation in the ZCE zone produces a high current for a very small thickness compared with that of the base. The total cell current is dominated by the diffusion photocurrent of the base, which accumulates with the photocurrent generated in the ZCE, increasing the total current. The heavily doped P+(Wbsf) layer boosts the total photocurrent of the bifacial cell from 28.8 to 31.8 mA/cm^2, A practical enhancement that will inspire further research and development in the field.

ACKNOWLEDGMENTS

For this paper, we do not have acknowledgement.

FUNDING INFORMATION

We do not have any funding.

AUTHOR CONTRIBUTIONS STATEMENT

This journal uses the Contributor Roles Taxonomy (CRediT) to recognize individual author contributions, reduce authorship disputes, and facilitate collaboration.

Name of Author	C	M	So	Va	Fo	I	R	D	O	E	Vi	Su	P	Fu
Seloua Bouchekouf	✓	✓	✓	✓	✓	✓		✓	✓	✓				
Hocine Guentri		✓				✓		✓	✓	✓		✓	✓	
Liamena Hassinet	✓					✓			✓		✓			
Amina Merzougui			✓	✓			✓		✓		✓			
Farida Kebaili		✓			✓		✓					✓		

C : **C**onceptualization
M : **M**ethodology
So : **So**ftware
Va : **Va**lidation
Fo : **Fo**rmal analysis
I : **I**nvestigation
R : **R**esources
D : **D**ata Curation
O : Writing - **O**riginal Draft
E : Writing - Review & **E**diting
Vi : **Vi**sualization
Su : **Su**pervision
P : **P**roject administration
Fu : **Fu**nding acquisition

CONFLICT OF INTEREST STATEMENT

There is no conflict of interest for this paper

INFORMED CONSENT

We did not introduce any personality into our study.

ETHICAL APPROVAL

In this paper, we have not mentioned either human beings or animals.

DATA AVAILABILITY

The data that support the findings of this study are available from the first author, SB, upon reasonable request.

REFERENCES

[1] S. Ishizuka, R. Okamoto, and S. Ikeda, "Enhanced performance of ternary CuGaSe2 thin-film photovoltaic solar cells and photoelectrochemical water splitting hydrogen evolution with modified p–n heterointerfaces," *Advanced Materials Interfaces*, vol. 9, no. 25, Sep. 2022, doi: 10.1002/admi.202201266.

[2] J. Yadav, J. Prasad, H. Sharma, S. Kumar, and M. Singh, "Effect of Zn and Sn incorporation on the crystallinity of spin-coated CuInSe2 thin films," *Journal of Materials Science: Materials in Electronics*, vol. 33, no. 24, pp. 19119–19128, Aug. 2022, doi: 10.1007/s10854-022-08749-x.

[3] Z. Zhang, S. Liu, and Y. Zhang, "Refining DIIS algorithms for Si and GaAs solar cells: incorporation of weight regularization, conjugate gradient, and reverse automatic differentiation techniques," *Physical Chemistry Chemical Physics*, vol. 26, no. 16, pp. 12717–12724, 2024, doi: 10.1039/D4CP00456F.

[4] M. J. Shin *et al.*, "Semitransparent and bifacial ultrathin Cu(In,Ga)Se2 solar cells via a single-stage process and light-management strategy," *Nano Energy*, vol. 82, p. 105729, Apr. 2021, doi: 10.1016/j.nanoen.2020.105729.

[5] B. Salhi, "The photovoltaic cell based on CIGS: Principles and technologies," *Materials*, vol. 15, no. 5, p. 1908, Mar. 2022, doi: 10.3390/ma15051908.

[6] A. F. Violas, A. J. N. Oliveira, P. A. Fernandes, P. M. P. Salomé, and J. P. Teixeira, "CIGS bifacial solar cells with novel rear architectures: Simulation point of view and the creation of a digital twin," *Solar Energy Materials and Solar Cells*, vol. 272, p. 112899, Aug. 2024, doi: 10.1016/j.solmat.2024.112899.

[7] A. Soheili, M. Hayati, and F. Shama, "Conversion efficiency improvement of CGS/CIGS photovoltaic cell," *Optik*, vol. 287, p. 171089, Sep. 2023, doi: 10.1016/j.ijleo.2023.171089.

[8] N. Mufti *et al.*, "Review of CIGS-based solar cells manufacturing by structural engineering," *Solar Energy*, vol. 207, pp. 1146–1157, Sep. 2020, doi: 10.1016/j.solener.2020.07.065.

[9] S. Rawat, R. Gupta, and S. Gohri, "Performance assessment of CIGS solar cell with different CIGS grading profile," *Materials Today: Proceedings*, Mar. 2023, doi: 10.1016/j.matpr.2023.03.356.

[10] D. Hariskos and M. Powalla, "Thermodynamic limitations for alkali metals in Cu(In,Ga)Se 2," *Journal of Materials Research*, vol. 32, no. 20, pp. 3789–3800, Oct. 2017, doi: 10.1557/jmr.2017.394.

[11] X. Yang, Ed., *Photoenergy and thin film materials*. Wiley, 2019. doi: 10.1002/9781119580546.

[12] X. Kong, Y. Yang, H. Zhang, Y.-H. Liu, and Y. Wang, "Advances in II–VI semiconductor magic-size clusters: Synthesis, characterization, and applications in nanotechnology," *Coordination Chemistry Reviews*, vol. 518, p. 216065, Nov. 2024, doi: 10.1016/j.ccr.2024.216065.

[13] A. Owens, "Photoconductive materials: Fundamentals, techniques and applications," in *Photoconductivity and Photoconductive Materials*, Wiley, 2022, pp. 399–491. doi: 10.1002/9781119579182.ch10.

[14] K. Benameur, Y. Mouchaal, K. Benchouk, A. Laafer, and R. Barille, "Syntheses and characterizations of CuIn1-xZnxSe2 chalcopyrite nanoparticles," *Materials*, vol. 15, no. 4, p. 1436, Feb. 2022, doi: 10.3390/ma15041436.

[15] I. Hamideddine, N. Tahiri, O. El Bounagui, and H. Ez-Zahraouy, "Theoretical investigation of electronic and optical properties of the CuIn1-x GaxSe2: Ab initio calculation," *Optik*, vol. 207, p. 163881, Apr. 2020, doi: 10.1016/j.ijleo.2019.163881.

[16] M. Ballabio, D. Fuertes Marrón, N. Barreau, M. Bonn, and E. Cánovas, "Composition-dependent passivation efficiency at the CdS/CuIn 1- x Ga x Se 2 interface," *Advanced Materials*, vol. 32, no. 9, Mar. 2020, doi: 10.1002/adma.201907763.

[17] V. Kumar, R. Prasad, N. B. Chaure, and U. P. Singh, "Advancement in Copper Indium Gallium Diselenide (CIGS)-based thin-film solar cells," *Advances in Sustainability Science and Technology*. Springer, Singapore, pp. 5–39. doi: 10.1007/978-981-19-3724-8_2.

[18] H. Elhosiny Ali, H. Algarni, I. S. Yahia, and Y. Khairy, "Optical absorption and linear/nonlinear parameters of polyvinyl alcohol films doped by fullerene," *Chinese Journal of Physics*, vol. 72, pp. 270–285, Aug. 2021, doi: 10.1016/j.cjph.2021.04.022.

[19] R. Prasad, A. K. Das, and U. P. Singh, "Bilayer CIGS-based solar cell device for enhanced performance: a numerical approach," *Applied Physics A*, vol. 127, no. 2, p. 140, Feb. 2021, doi: 10.1007/s00339-021-04298-y.

[20] S. R. I. Biplab, M. H. Ali, M. M. A. Moon, M. F. Pervez, M. F. Rahman, and J. Hossain, "Performance enhancement of CIGS-based solar cells by incorporating an ultrathin BaSi2 BSF layer," *Journal of Computational Electronics*, vol. 19, no. 1, pp. 342–352, Mar. 2020, doi: 10.1007/s10825-019-01433-0.

[21] J. Ji, G. Yu, C. Xu, and H. J. Xiang, "General theory for bilayer stacking ferroelectricity," *Physical Review Letters*, vol. 130, no. 14, p. 146801, Apr. 2023, doi: 10.1103/PhysRevLett.130.146801.

[22] A. Ghobadi, M. Yousefi, M. Minbashi, A. H. A. Kordbacheh, A. R. H. Abdolvahab, and N. E. Gorji, "Simulating the effect of adding BSF layers on Cu2BaSnSSe3 thin film solar cells," *Optical Materials*, vol. 107, p. 109927, Sep. 2020, doi: 10.1016/j.optmat.2020.109927.

[23] E. Yükseltürk, O. Surucu, M. Terlemezoglu, M. Parlak, and Ş. Altındal, "Illumination and voltage effects on the forward and reverse bias current–voltage (I-V) characteristics in In/In2S3/p-Si photodiodes," *Journal of Materials Science: Materials in Electronics*, vol. 32, no. 17, pp. 21825–21836, Sep. 2021, doi: 10.1007/s10854-021-06378-4.

[24] W. Gu, T. Ma, M. Li, L. Shen, and Y. Zhang, "A coupled optical-electrical-thermal model of the bifacial photovoltaic module," *Applied Energy*, vol. 258, p. 114075, Jan. 2020, doi: 10.1016/j.apenergy.2019.114075.

[25] F. Li, L. Cheng, J. Fan, and Q. Xiang, "Steering the behavior of photogenerated carriers in semiconductor photocatalysts: a new insight and perspective," *Journal of Materials Chemistry A*, vol. 9, no. 42, pp. 23765–23782, 2021, doi: 10.1039/D1TA06899G.

[26] D. Wang *et al.*, "Bidirectional photocurrent in p–n heterojunction nanowires," *Nature Electronics*, vol. 4, no. 9, pp. 645–652, Sep. 2021, doi: 10.1038/s41928-021-00640-7.

[27] D. Xia, J. Li, M. Xu, and X. Zhao, "Electrodeposited and selenized CIGS thin films for solar cells," *Journal of Non-Crystalline Solids*, vol. 354, no. 12–13, pp. 1447–1450, 2008, doi: 10.1016/j.jnoncrysol.2007.02.097.

BIOGRAPHIES OF AUTHORS

Seloua Bouchekouf obtained her degree in electronics engineering with a communication option from the University of Constantine, Algeria, in 1999 and her degrees of Magister and Doctorate in science in electronics specializing in semiconductors and electronic systems from the same University, in 2004 and 2010, respectively. She was a teacher at the Abdelhak Ben Hammouda University Jijel in Algeria between 2011-2015. Currently, she is associated with the Department of Mechanical and Electromechanical Engineering of the Abdelhafid Boussouf Mila University Center in Algeria. Her research areas include renewable energy, photovoltaic cells, and energy production. She can be contacted at email: s.bouchecouf@centre-univ-mila.dz.

Hocine Guentri was born on 19.06.1973. In 1996, he graduated from the Department of Electrotechnics of the Faculty of Electrical Engineering at the University Ibn Khaldun in Algeria. The master's degree from the University of Saida Algeria. The PhD degree from the University of Sidi Bel-Abbes, Algeria, in 2018. His research activities primarily concentrate on power systems, FACTS, renewable energy, and sustainable energy, and his research activities focus on smart grid systems and storage hybrid systems. He is a lecturer at the University Centre Nour Bachir El Bayadh in Algeria. He can be contacted at email: h.guentri@cu-elbayadh.dz

Liamena Hassinet obtained her degree in mechanical engineering from the University of Batna, Algeria, in 1993 and her degrees of magister and doctorate in science in mechanics specializing in energy, from the same university, in 2008 and 2018. Her affiliation is with the Department of Mechanical and Electromechanical Engineering of Abdelhafid Boussouf Mila University Center in Algeria. Her research areas include heat transfer, fluid mechanics, and energy production. She can be contacted at email: hassinet@centre-univ-mila.dz.

Amina Merzougui obtained her degree in electronics engineering with an instrumentation option from the University of Constantine, Algeria, in 1999 and her degrees of magister and doctorate in science in electronics from the same university, in 2004 and 2010, respectively. She was a teacher at the Abdelhak Ben Hammouda University Jijel in Algeria between 2011-2016. Currently, she is associated with Institute of Applied Science and Technology in Oum El Bouaghi university Algeria. Her current position is department head of the same Institute. She can be contacted at email: merzougui3amina@gmail.com.

Farida Kebaili obtained her baccalaureate in 1994. She earned her master's degree in 2002 from the University of Frères Mentouri, Constantine1, with a thesis entitled “Analytical modeling of MESFET operation in GaAs”. She received her PhD in 2010 with a dissertation on “Numerical physical modeling of MESFET and CNTFET structures”. She has been a lecturer and researcher at the University of M’sila since 2008. Her current research focuses on photonic crystals, with several scientific publications in this field. She can be contacted at email: farida.kebaili@univ-msila.dz.